Marine and Petroleum Geology 89 (2018) 202–215

Contents lists available at ScienceDirect

Marine and Petroleum Geology

journal homepage: www.elsevier.com/locate/marpetgeo

Research paper

Hydrocarbon source for oil and gas indication associated with gas hydrate and its significance in the Qilian Mountain permafrost, Qinghai, Northwest China

Bin Cheng [a], Jianbing Xu [a, e], Zhenquan Lu [b, **], Yonghong Li [c], Weichao Wang [c], Shan Yang [a], Hu Liu [a, d], Ting Wang [b], Zewen Liao [a, *]

[a] State Key Laboratory of Organic Geochemistry, Guangzhou Institute of Geochemistry, Chinese Academy of Sciences, Guangzhou 510640, China
[b] Oil & Gas Survey, China Geological Survey, Beijing 100029, China
[c] Qinghai No.105 Coal Geological Exploration Team, Xining 810007, China
[d] Sichuan Key Laboratory of Shale Gas Evaluation and Exploitation, Chengdu 600091, China
[e] University of Chinese Academy of Sciences, Beijing 100049, China

ARTICLE INFO

Article history:
Received 4 October 2016
Received in revised form
13 February 2017
Accepted 16 February 2017
Available online 21 February 2017

Keywords:
Gas hydrate
Oil and gas indication
Oil (gas)-source correlation
Qilian Mountain permafrost

ABSTRACT

Since gas hydrate was sampled by drilling in the Qilian Mountain permafrost in 2008, to investigate the source of the gas hydrate and the relationship between gas hydrate and the concomitant oil and gas indication (OGI) have become an important research focus. The rocks bearing gas hydrate and OGI from the Middle Jurassic strata in the Qilian Mountain permafrost, Qinghai, Northwest China were extracted by organic solvent and thermally treated (300 °C and 400 °C) in vacuum glass tubes. The hydrocarbons from the extracts and cracked products of the rocks and the stable carbon isotope of the gas hydrocarbons were studied. The results showed that the OGIs can be classified into two types according to different biomarker characteristics. The I-type of OGIs, which suffered from the process of early biodegradation and later-hydrocarbon input and featured high concentrations of 17α(H)-diahopane and αββ-regular steranes, mainly originated from the shallow source rocks of the Middle Jurassic strata, while the II-type one with a series of long-chain alkylnaphthalene may originate from the lower portion of Middle Jurassic or deeper source rocks than the Middle Jurassic strata. The adsorbed gas (300 °C) of the Middle Jurassic rocks was very wet, had a normal carbon isotope sequence, and can be regarded as an organic thermogenic gas derived from Middle Jurassic source rocks. Comparing the adsorbed (300 °C) and cracked (400 °C) gases from the rocks with gases from the gas hydrate and drilling core, we found they had similar stable carbon isotope distributions but different relative contents of methane (C_1), ethane (C_2), and propane (C_3). The Middle Jurassic source rocks are mainly deposited in a freshwater paleo-environment, similar to the parent biomass of the gas hydrate and drilling core gas. The difference of the relative concentrations of C_1-C_3 may result from different formation processes between the adsorbed and cracked gases and the gas hydrate and drilling core gas. The II-type OGI, which possibly originated from deeper strata than the Middle Jurassic, were closely associated with the gas hydrate under the drilling well and had a similar parent biomass and depositional environment as the gas hydrate, showing they have a closely correlated hydrocarbon origin.

1. Introduction

Gas hydrate is a white crystal formed by water and light gases (such as CH_4, C_2H_6, C_3H_8, i-C_4H_{10}, H_2S, and CO_2) under low temperature (around 273.15 K) and high pressure (3–5 MPa) conditions (Sloan and Koh, 2008), which is mainly found in deep ocean sediments and terrestrial permafrost zones. Gas hydrate has attracted widespread attention by many researchers since mid-1990 (Moridis et al., 2011; Ruppel, 2011; Lu, 2015) because of its huge energy potential as a new type of clean energy (Milkov, 2004; Boswell and Collett, 2011).

Since gas hydrate was first sampled from wells DK-1, DK-2, and DK-3 in the Qilian Mountain permafrost in 2008 (Lu et al., 2011),

* Corresponding author.
** Corresponding author.
E-mail addresses: luzhq@vip.sina.com (Z. Lu), zw_liao@hotmail.com (Z. Liao).

http://dx.doi.org/10.1016/j.marpetgeo.2017.02.019
0264-8172/

more gas hydrate samples have been found in wells DK-7, DK-8, DK-9, DK-12, DK13-11, DK12-13, DK11-14, and DK8-19, as well as abnormal phenomenon associated with gas hydrate in some other wells (Lu et al., 2015a), indicating the Qilian Mountains permafrost area has favorable geological conditions, such as sufficient hydrocarbon gas sources, qualified temperature and pressure background, for the formation of gas hydrate (Zhu et al., 2006). The gas hydrate inside which the natural gas has CH_4 content of 54%–76%, C_2H_6 of 8%–15%, and C_3H_8 of 4%–21%, generally occurs in mudstones, oil shales, and sandstones 133–396 m deep (Zhu et al., 2010). Prior studies on gas compositions and their stable carbon isotopes from gas hydrate, drilling core gas, and headspace gas suggested that the gases from gas hydrate were mainly organic thermogenic (Huang et al., 2011; Lu et al., 2013a, 2015a,b; Tang et al., 2015), partially mixed with microbial and thermogenic (Wang et al., 2015), and originated from sapropelic source rock deposited in a freshwater environment (Liu et al., 2012; He et al., 2015). Additionally, inside the rocks from the drilling core bearing gas hydrate in the Qilian Mountain permafrost, Lu et al. (2013a) found a significant amount of oil and gas indication (OGI) phenomena, such as oil trace, oil patch, oil immersion, and oil staining, and thought their presence was closely associated with gas hydrate. These OGIs were mainly composed of intermediate-weighted oil with a small amount of heavy oil, over-heavy oil, and even asphalt, which has been suggested as a sign for gas hydrate occurrence (Lu et al., 2013a,b).

The generation mechanism for the hydrocarbon gases of gas hydrate from the Qilian Mountain permafrost was mainly organic and thermogenic, for which the majority of studies agree. However, the specific origination of the hydrocarbon gases is still unclear because we lack an accurate correlation from gas to source. In essence, the OGIs were closely associated with the gas hydrate and are considered a sign of gas hydrate occurrence, but a study about its hydrocarbon composition and origination has been not reported so far. Therefore, this paper focuses on the geochemical characteristic of OGIs and absorbed and cracked gases from the rock and carries out the oil (gas)-source correlation based on the hydrocarbon composition and its stable carbon isotope distribution, which is helpful in understanding the relationship between the hydrocarbons from OGIs and gas hydrate and the Middle Jurassic source rocks and the relationship between OGI and gas hydrate.

2. Geological setting

Qilian Mountain is located in the north Qinghai Tibet Plateau and consists of Zoulangnan Mountain (North Qilian structural zone), Tuolai Mountain (Middle Qilian block), and the South Qilian structural zone. In the early Paleozoic, the South Qilian basin was a small ocean basin between the Qaidam Block and the North China Block. The ocean basin closed, began to uplift, and suffered erosion under the effect of the Caledonian Movement in the late Silurian (Fu and Zhou, 1998). During the Carboniferous, the basin began to sink and formed a wide shallow-marine shelf facies depositional environment; due to different tectonic evolution in the Permian, the North Qilian basin was uplifted, while the South Qilian basin remained a shallow-marine shelf or epicontinental sea environment; the South Qilian basin was still an ocean basin in the Triassic and deposited a set of marine sandy mudstone clip limestones (Fu and Zhou, 1998). However, the whole Qilian area was uplifted when the Paleo-Tethys Ocean closed under the influence of the Indosinian Movement in the terminal of the Late Triassic (Fu and Zhou, 1998). In the early Cretaceous, the South Qilian Block was rapidly cooling and suffered from erosion with the Qilian Mountain uplifting; since the Miocene, the Qilian Mountain has experienced north-eastward rise and growth, forming basin-mountain tectonic landforms (Qi et al., 2016).

The South Qilian Basin, located in the South Qilian tectonic belt, is thought to be rich in oil and gas and can be subdivided into five secondary depressions: Shule Depression, Muli Depression, Halahu Depression, Xiariha Depression, and Tianjun Depression (Fu and Zhou, 1998) (Fig. 1a). In the Muli Depression, there are four good source rocks, referred to as Carboniferous dark mudstone (limestone), Caodigou Formation dark limestone from the Lower Permian, Galedeshi Formation dark mudstone from the upper Triassic, and Jurassic dark shale. Due to these source rocks being excellent in hydrocarbon generation and mature-over mature thermal evolution stage, the South Qilian Basin is regarded as one of greatest potential depressions for oil and gas exploration (Fu and Zhou, 1998).

The study area is located within the Juhugeng mining district, Muli coalfield in the Northwest Muli Depression, administratively belonging to Muli town, Tianjun county in Qinghai Province. This area mainly exposes the Upper Triassic, Quaternary, and Middle Jurassic strata (Fig. 1b). The Middle Jurassic strata (Fig. 2), a coal-bearing clastic rock, consists of a suite of fluvial, lacustrine, and swamp facies sediments (Wen et al., 2006). The Middle Jurassic source rock from the Juhugeng mining district included the Muli Formation (J_2m) and the Jiangchang formation (J_2j) from bottom to top. The Muli formation is mainly a braid-shaped river, lacustrine, and swamp facies sediment, with sandstone and coal line, while the Jiangchang Formation is a delta-lacustrine facies sediment and contains mudstone, oil shale, and sandstone (Lu et al., 2015a,b; Tang et al., 2015). The gas hydrate and abnormal phenomenon associated with gas hydrate were found in the Muli Formation and the Jiangchang Formation (Lu et al., 2010, 2013a,b).

3. Materials and experiment

3.1. Samples and their pre-treatment

Rock samples, including sandstone, mudstone, oil shale, and limestone, were collected from the Middle Jurassic strata bearing gas hydrate from wells DK9, DK10-16, DK11-14, DK12-13, and DK13-11 in the Qilian Mountain permafrost area (Figs. 1b and 3). The five wells are all located at the Sanlutian bare field of the Juhugeng Coalmine Area in Qinghai Province. The horizontal distance between these wells is very small, with a maximum distance around 1 km (Lu et al., 2015a). Details about the well sites are in Fig. 1b.

Sandstone samples marked DK9-O-01, DK9-O-09, DK9-O-18, and DK9-O-19 from DK9 well, bear OGI phenomena such as oil trace, oil patch, oil immersion, and oil staining. The other samples from DK9 well were mudstones and oil shales and used for releasing adsorbed and cracked hydrocarbons from the rock. The samples of mudstone, argillaceous sandstone, or sandy mudstone in wells DK10-16, DK11-14, DK12-13, and DK13-11 were used for releasing cracked gas from kerogen or residual organisms. A previous study showed that the source rocks from wells DK2 and DK3 in the Qilian Mountain permafrost basically did not undergo thermal pyrolysis at 300 °C but would release cracked gas at 400 °C when they were warmed in the closed glass tube systems (Lu et al., 2013c). Therefore, the temperatures 300 °C and 400 °C are selected for heating the samples in the closed glass tube systems to release the adsorbed and cracked gases.

All rock samples are milled into powder and then treated using the following steps: (1) the mudstone and oil shale samples are analyzed by utilizing a Rock-Eval 6.0 Standard Pyrolysis Analyzer to obtain the basic pyrolysis data. (2) All samples are extracted for 120 h with dichloromethane to obtain the soluble fractions of the rocks. The residues are pyrolyzed at 400 °C for 72 h in the closed glass tube systems, obtaining cracked gas from kerogen or residual organic matter. (3) The soluble components from the DK9 well

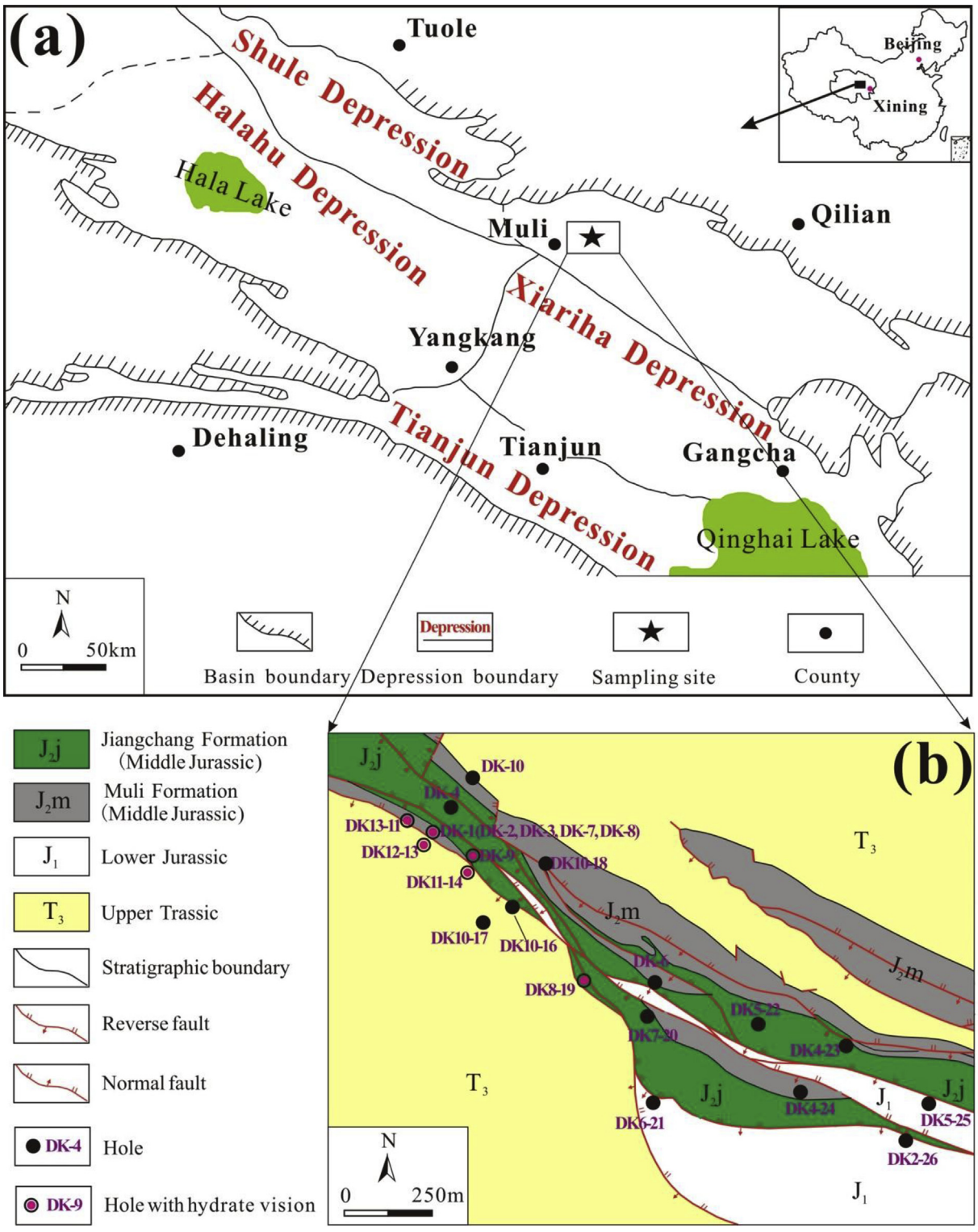

Fig. 1. Depressions in the South Qilian Basin (a) (From Fu and Zhou, 1998, with minor modification) and drilling location (b) (From Lu et al., 2015a, with modification).

samples were further fractionated by column chromatography on silica/alumina (2:1, v/v) and eluted using *n*-hexane and toluene to obtain the saturated and aromatic hydrocarbon fractions. (4) The 400 °C pyrolysis residues from DK9 well in step 2 are extracted for 120 h with dichloromethane. The extracted fractions were further fractionated to obtain the saturated and aromatic hydrocarbon fractions, similar to step 3. (5) Part of the dichloromethane extracted samples (residues) from DK9 well are heated to 300 °C for 72 h in the closed glass tube systems, to obtain the adsorbed gas from the rock.

3.2. Instrumental analysis

Rock pyrolysis analyses are performed on a Rock-Eval 6.0

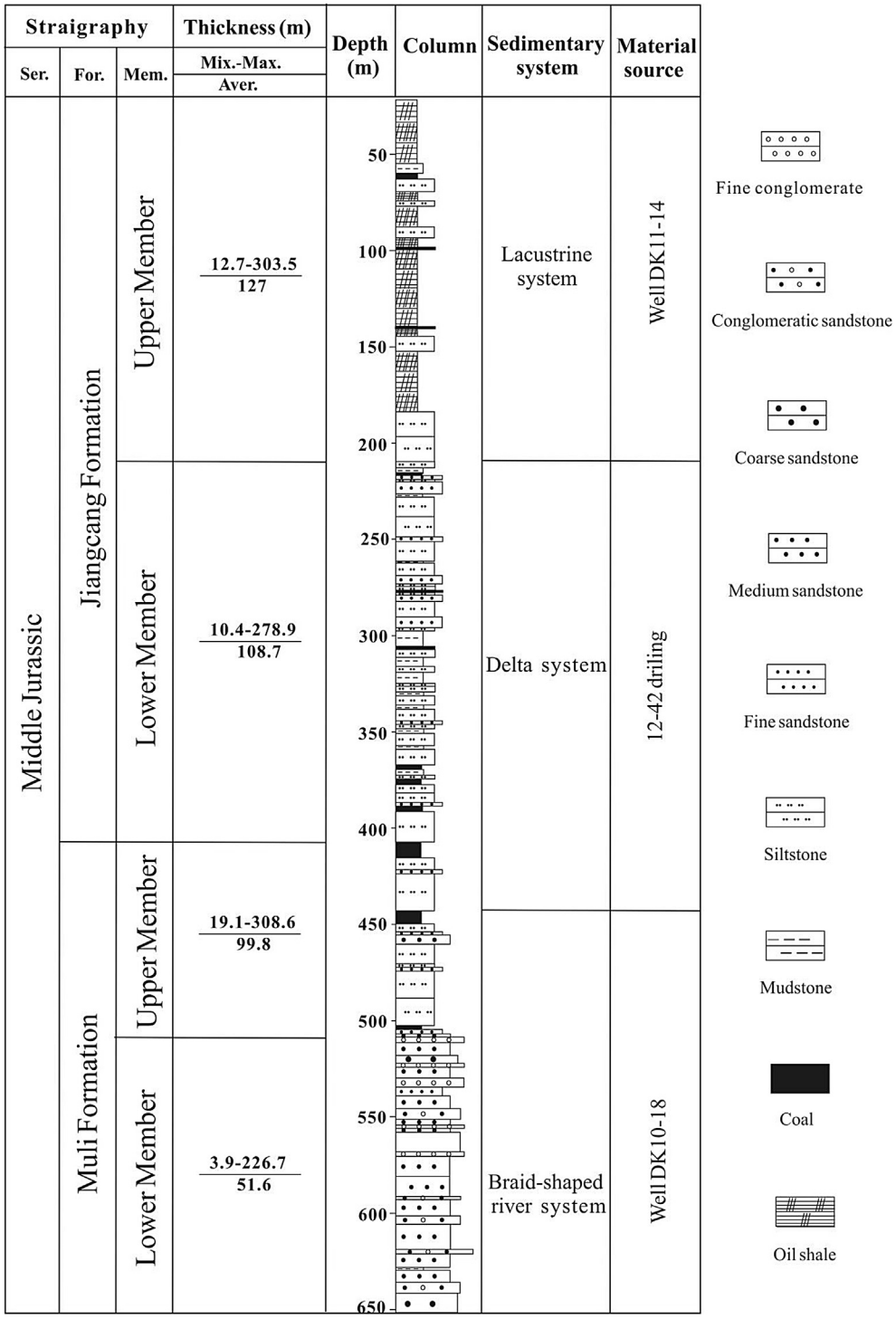

Fig. 2. Stratigraphy section showing sedimentary facies of the Middle Jurassic in the Juhugeng mining district (From Yang et al., 2015, with modification).

Standard Pyrolysis Analyzer. Gas component analysis was done on a two-channel Hewlett–Packard 6890 gas chromatography (GC) made by the company of Wassen ECE. The analysis of the gas stable carbon isotope was done on a HP 5890 GC interfaced to a VG Isochrom II mass spectrometer.

Analysis of liquid hydrocarbons was done on a DSQ II and Trace GC Ultra combined system from Thermo Fisher. GC conditions were: HP-1MS chromatographic column (60 m × 0.32 mm × 0.25 μm) with helium as carrier gas with a constant flow mode at 1.2 mL/min. Mass spectrometry (MS) conditions were: electron impact (EI) mode; ion source electron energy, 70 eV; ion source temperature, 260 °C; and mass scan range, 50–650 Da. The temperature ramp-up procedure for the saturated hydrocarbons was as follows: an initial temperature of 80 °C was held for 4 min then raised to 295 °C at a rate of 4 °C/min and held for 20 min. The temperature ramp-up procedure for the aromatic hydrocarbons was as follows: an initial temperature of 80 °C was held for 4 min then raised to 295 °C at a rate of 3 °C/min and held for 30 min.

Fig. 3. Photos of drilling core samples. (a)Sandstone bearing OGI; (b) Mudstone; (c) limestone; (d) Sandstone without OGI.

4. Results and discussion

4.1. Rock-eval analysis

The samples detected by Rock-Eval 6.0 Standard Pyrolysis Analyzer were mudstones and oil shales from 169.56 m to 378.10 m depth in wells DK9, DK10-16, and DK11-14 (Table 1). The results show that almost all of the source rocks have a maximum temperature (Tmax) of 440–450 °C and PI < 0.1, indicating those samples were in the low–mature stage. Their TOC (total organic carbon) contents are beyond 1.34% and the highest one (DK9-O-12) even reached 12.04%, indicating a significant amount of organic matter. The content of free hydrocarbons (S1) of those rocks ranged from 0.16 mg/g to 3.37 mg/g, while that of the cracked hydrocarbons (S2) ranged from 1.50 mg/g to 106.3 mg/g. We observed that those samples are all distributed in the area of excellent source rocks in the TOC- (S1+S2) (Fig. 4-a). The source rocks are predominantly type I–II kerogens according to the Tmax-HI diagram (Fig. 4-b).

4.2. Parent origination analysis of OGI

4.2.1. Organic geochemistry characteristic of OGI

The content of dichloromethane extracts from sandstones bearing OGI and the relative concentrations of the saturated hydrocarbon, aromatic hydrocarbon, and non-hydrocarbon from extracts are listed in Table 2. In sample DK9-O-01, the extract content was only 0.17%, in which the order for relative concentration of each fraction was aromatic hydrocarbon < saturated hydrocarbon ≤ non-hydrocarbon, with non-hydrocarbon concentrations of up to 78.5%. However, the dichloromethane extracts of the other sandstones were different from DK9-O-01. Their extracts had contents ranging from 0.84% to 2.41% and the order non-hydrocarbon < aromatic hydrocarbon ≤ saturated hydrocarbon for relative concentrations, with saturated hydrocarbon contents of up to 66.5%–81.6%.

4.2.1.1. Saturated hydrocarbon. On the total ion chromatogram (TIC) of saturated hydrocarbon (Fig. 5), the *n*-alkanes in the four OGI samples showed a unimodal distribution and their dominant *n*-alkane ranged from C_{20} to C_{23}. The DK9-O-01 sample had different *n*-alkane distribution features, with details as follows: the *n*-alkanes of DK9-O-01 exhibited certain "unresolved complex mixture" (UCM) peaks on the chromatograms and their carbon numbers ranged from C_{16} to C_{31}, with a Pr/Ph ratio of 1.42 (Table 3). However, it was difficult to observe the UCM peaks on the TIC chromatograms of the other three samples. They had *n*-alkane carbons of C_{12}-C_{36} and a Pr/Ph ratio of 0.92.

Table 1
Rock-Eval results of the Middle Jurassic source rock in the Qilian Mountain permafrost.

Samples	Depth (m)	Lithology	S1 (mg/g)	S2 (mg/g)	S1+S2 (mg/g)	PI	Tmax (°C)	HI (mg/g)	OI (mg/g)	TOC (wt %)
DK9-O-02	169.56	Mudstone	0.39	12.27	12.66	0.03	449	371	5	3.31
DK9-O-04	200.15	Mudstone	0.16	3.21	3.37	0.05	443	240	8	1.34
DK9-O-05	204.47	Mudstone	0.28	5.39	5.67	0.05	443	257	3	2.10
DK9-O-06	204.57	Mudstone	0.47	6.31	6.78	0.07	442	305	4	2.07
DK9-O-07	209.12	Mudstone	0.59	10.58	11.17	0.05	445	334	2	3.17
DK9-O-08	225.34	Mudstone	0.77	32.35	33.12	0.02	450	703	/	4.60
DK9-O-10	249.12	Mudstone	0.96	7.22	8.18	0.12	438	372	3	1.94
DK9-O-11	258.70	Mudstone	1.41	18.95	20.36	0.07	443	793	5	2.39
DK9-O-12	268.70	Oil shale	2.46	106.3	108.8	0.02	449	883	1	12.04
DK9-O-13	270.47	Mudstone	3.37	64.76	68.13	0.05	449	888	/	7.29
DK9-O-14	285.49	Mudstone	0.45	3.08	3.53	0.13	440	177	29	1.74
DK9-O-15	288.54	Mudstone	0.29	1.50	1.79	0.16	440	82	137	1.82
DK9-O-16	301.68	Mudstone	0.24	6.74	6.98	0.03	448	465	6	1.45
DK10-16-3	325.70	Mudstone	3.31	46.36	49.67	0.07	447	797	/	5.82
DK11-14-4	378.10	Mudstone	2.7	18.13	20.83	0.13	443	514	/	3.53

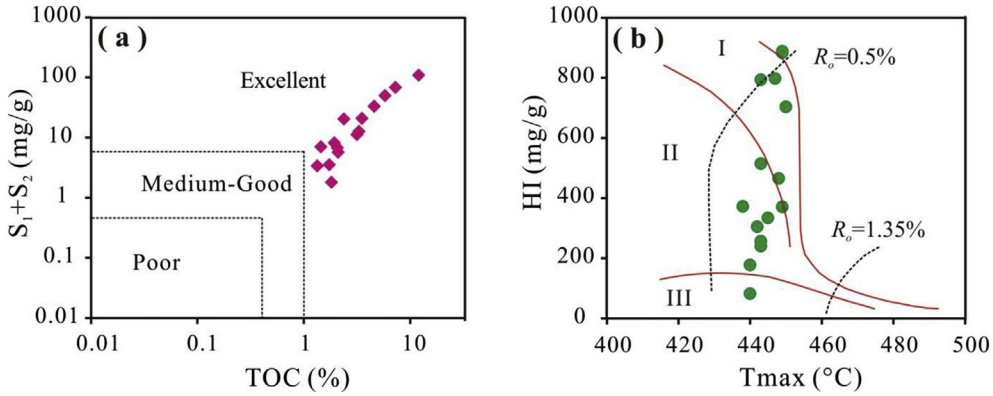

Fig. 4. The diagrams of TOC-(S1+S2)(a) (reference Gao et al., 2016) and Tmax-HI (b) (reference Peng et al., 2016).

Table 2
The relative concentrations of extracts and their fractions for OGI from the DK-9 well.

Samples	Depth (m)	Extract (wt%)	S (%)	A (%)	N (%)
DK9-O-01	160.51	0.17	12.2	9.2	78.5
DK9-O-09	237.15	2.41	81.6	17.3	1.0
DK9-O-18	360.93	0.84	66.5	20.9	12.6
DK9-O-19	366.90	1.53	66.7	20.0	13.3

Note: Extract: dichloromethane extract; S: saturated hydrocarbon; A: aromatic hydrocarbon; N: non-hydrocarbon.

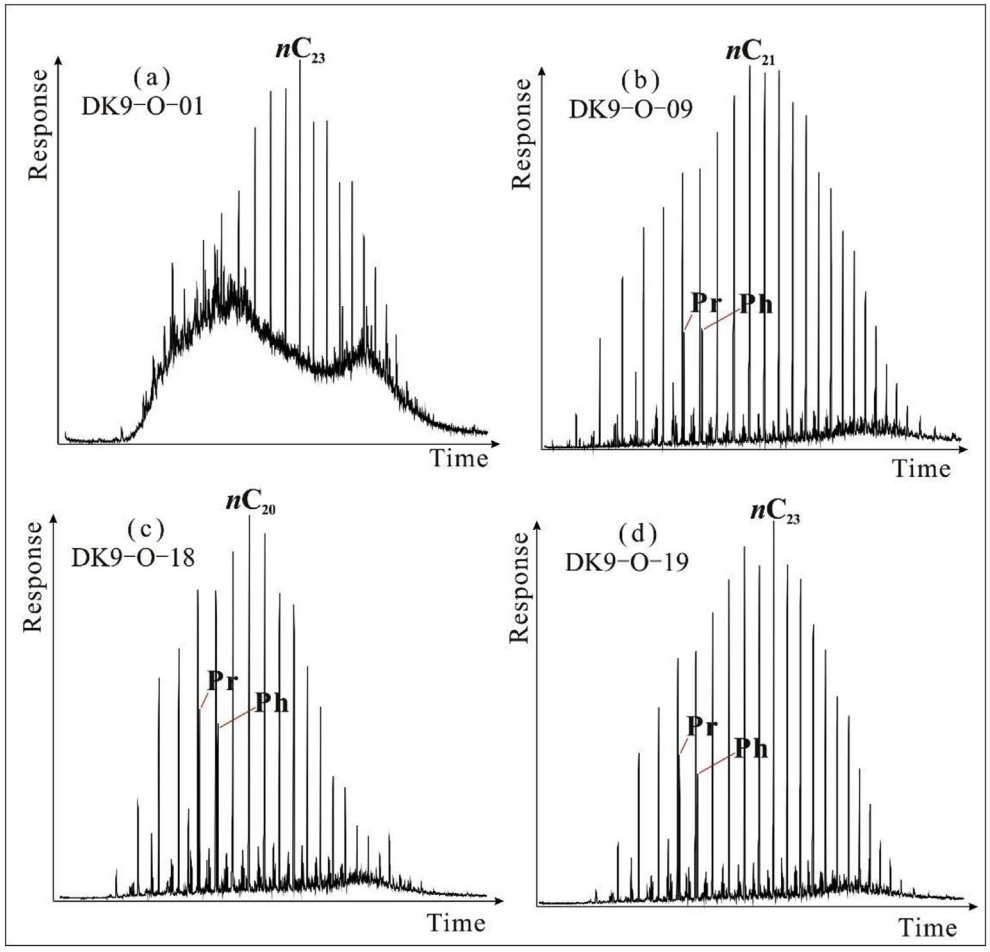

Fig. 5. Chromatograms of the saturated hydrocarbon from OGI. The biomarker assignments are listed in Table 4.

Table 3
Biomarker parameters of OGI samples from DK-9 well.

Samples	Pr/Ph	Ts/(Ts + Tm)	C_{30}RH/C_{29} (H + Ts)	$C_{20\text{-}21}$P/ $C_{27\text{-}29}$S	C_{27}D/ $C_{27\text{-}29}$S	C_{27}DS/ (S + R)	C_{27}ααα R/ C_{27}S	C_{28}ααα R/ C_{28}S	C_{29}ααα R/ C_{29}S	C_{29}S/ (S + R)	C_{29}Sββ/ (αα+ββ)
DK9-O-01	1.42	0.52	0.51	0.14	0.34	0.57	0.08	0.06	0.13	0.60	0.68
DK9-O-09	0.92	0.44	0.09	0.02	0.05	0.53	0.29	0.34	0.32	0.45	0.41
DK9-O-18	1.06	0.42	0.08	0.02	0.10	0.54	0.25	0.31	0.29	0.50	0.43
DK9-O-19	1.11	0.41	0.07	0.03	0.11	0.54	0.26	0.32	0.29	0.49	0.42

Note: C_{30+RH}/C_{29}(H + Ts):17α(H)-diahopane/(17α,21β(H)-30-norhopane+18α(H)-30-norneohopane); $C_{21\text{-}22}$P/$C_{27\text{-}29}$S: (pregnane + homo-pregnane)/$C_{27\text{-}29}$ regular sterane; C_{27}D/$C_{27\text{-}29}$S:C_{27} diacholestane/C_{27}-C_{29} regular sterane; C_{27}D-S/(S + R): C_{27} diacholestane-20S/(20S + 20R); C_{27}ααα R/C_{27}S:C_{27}ααα R/C_{27} regular sterane; C_{28}ααα R/C_{28}S: C_{28}ααα R/C_{28} regular sterane; C_{29}ααα R/C_{29}S: C_{29}ααα R/C_{29} regular sterane; C_{29}S/(S + R): ααC_{29} regular sterane-20S/(20S + 20R); C_{29}S-ββ/(ββ+αα): C_{29} regular sterane-ββ/(ββ+αα).

Table 4
Biomarker assignments for the peaks in Figs. 4–8.

Peak	Compound
nC_{20}, nC_{21}, nC_{23}	C_{20}, C_{21}, C_{23} normal alkanes
Pr, Ph	Pristane and Phytane
C_{19}T, C_{24}T	C_{19}, C_{24} tricyclic terpanes
C_{24}Tet	C_{24} tetracyclic terpanes
Ts	22,29,30-Trisnorneohopane-II
Tm	22,29,30-Trisnorneohopane
C_{29}H	C_{29} 17α,21β(H)-30-norhopane
C_{29}Ts	C_{29} 18α(H)-30-norhopane
C_{30}H	C_{30} 17α,21β(H) hopane
C_{30}RH	17α(H)-diahopane
C_{31}H	C_{31} 17α,21β(H) 22S and 22R homo-hopane
C_{27}DS, C_{27}DR	C_{27} 13β, 17α 20S and 20R Diasteranes
C_{21}P	Pregnane
C_{27}S ~ C_{29}S	C_{27} ~ C_{29} Regular Sterane
AB	Alkylbenzene
P	Phenanthrene
(3-, 2-, 9-, 1-)MP	(3-, 2-, 9-, 1-)Methylphenanthrene
DP	Dimethylphenanthrene
TS	Triaromatic Sterane
C_4H_9-N	C_4H_9-Naphthalene
C_4H_9-D	C_4H_9-Diphenyl
C_2H_5-P	C_2H_5-Phenanthrene
C_{20}AN	C_{20}-Alkylnaphthalene

For the terpanes (Fig. 6), the hopanes were the main components compared to the tricyclic terpanes (C_{19}-C_{24}). The C_{30} hopane was the main peak and the relative abundance of the homohopane series decreased as the carbon number increased. It is notable that 17α(H)-diahopane (C_{30}RH) and 18α(H)-30-norhopane (C_{29}Ts) were detected in the four OGIs and the C_{29}Ts was co-eluted with C_{29} 17α,21β(H)-30-norhopane. However, the DK9-O-01 OGI had higher ratios of tricyclic terpanes/pentacyclic terpanes, C_{30}R/C_{29}(H + Ts), and Ts/(Ts + Tm) than the other OGI samples. The ratios of C_{30}R/C_{29}(H + Ts) and Ts/(Ts + Tm) from DK9-O-01 OGI were both 0.51 (Table 3).

For the steranes (Fig. 6), the regular steranes featured a V-type or asymmetrical V-type distribution. C_{27} 13β, 17α-diasteranes contained 20S and 20R isomers, and the relative concentration of the 20S isomer was higher than that of the 20R one. However, there were some differences between the DK9-O-01 OGI and the other three samples: (1) For the $C_{27\text{-}29}$ regular steranes, the ααα isomers from DK9-O-01 OGI had lower concentration than their αββ ones but opposite results were observed in the other OGIs (Table 3). For example, the ratio of C_{27}ααα R/C_{27} regular sterane in the DK9-O-01 OGI was 0.08, while that of the other three OGIs ranged from 0.25 to 0.29. (2) The maturity parameters, the C_{29}-ββ/(αα+ββ) and C_{29}-20S/(20S + 20R), from DK9-O-01 OGI were both higher than the other OGIs. For example, the DK9-O-01 OGI had a C_{29}-20S/(20S + 20R) ratio of 0.6, but the other OGIs had ratios of 0.45–0.50. (3) The ratio of C_{27} diacholestane/C_{27}-C_{29} regular sterane in DK9-O-01 OGI was

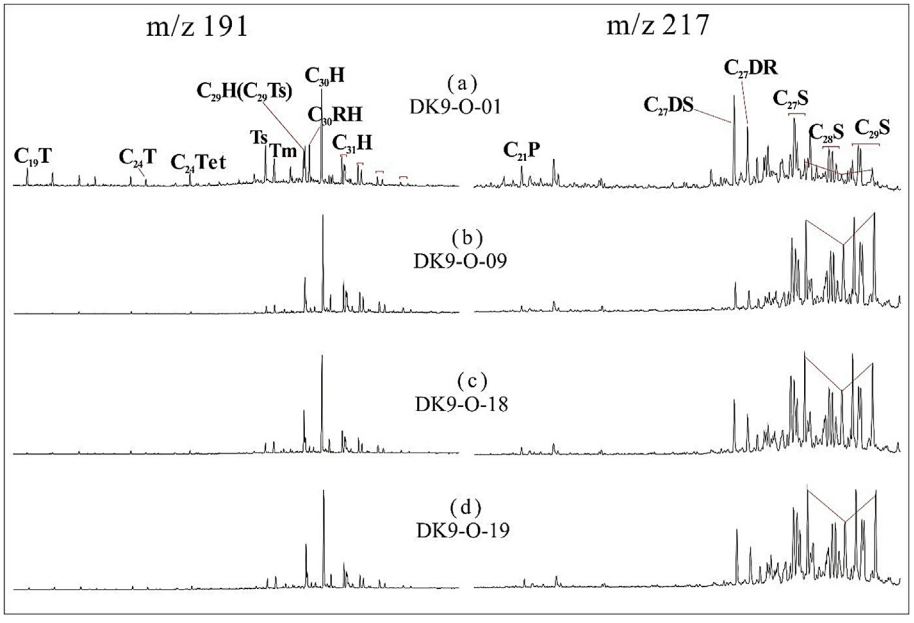

Fig. 6. Chromatograms of the terpanes and steranes from OGI. The biomarker assignments are listed in Table 4.

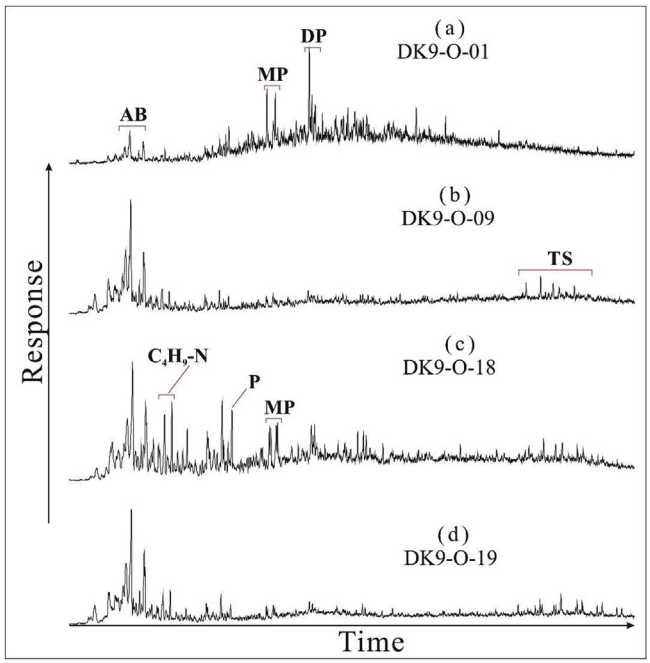

Fig. 7. Chromatograms of the aromatic hydrocarbon from OGI. The biomarker assignments are listed in Table 4.

0.34, but this ratio in the other three OGIs was 0.0–0.11, which is significantly lower.

4.2.1.2. Aromatic hydrocarbon. On the TIC chromatogram of aromatic hydrocarbon (Fig. 7), short chain alkylbenzene, C_4H_9-Naphthalene, phenanthrene, and methylphenanthrene were detected. Some triaromatic steranes (TS) were even visible in OGI samples DK9-O-09, DK9-O-018, and DK9-O-09. For some aromatic hydrocarbons, such as long chain alkylnaphthalene and methylphenanthrene, the three samples had similar distribution characteristics, though they were different from DK9-O-01.

On the m/z192 chromatogram of aromatic hydrocarbon (Fig. 8), 2-Methylphenanthrene and 9-Methylphenanthrene were dominant peaks in the OGI samples from DK9-O-09, DK9-O-018, and DK9-O-09, but the two component peaks were the lowest for the OGI from DK9-O-01. The {(2-MP)+(9-MP)}/{(1-MP)+(3-MP)} (M value for short) ratio was calculated and the result showed that the M value in DK9-O-01 was <1, while this value was >1 in the other samples. On the m/z142 chromatogram (Fig. 8), a series of long chain alkylnaphthalenes, with carbon numbers ranging from C_{14} to C_{33}, was detected in the DK9-O-09, DK9-O-18, and DK9-O-19 samples. These kinds of components contained two isomers, α-alkylnaphthalene and β-alkylnaphthalene. The α-alkylnaphthalene had a longer retention time in the chromatographic column and a higher concentration than those of the β-alkylnaphthalene. However, no long chain alkylnaphthalene was found in the DK9-O-01 OGI.

4.2.1.3. Origination and classification of OGI. Prior research showed that the shorter chain *n*-alkanes (C_{17}-C_{21}) have been thought to originate from marine phytoplankton and microbes (Blumer et al., 1971; Cranwell et al., 1987; Silliman and Schelske, 2003), and the medium chain *n*-alkanes (C_{23}-C_{27}) are generally considered to be derived from macroscopic algae (Ficken et al., 2000; Mead et al., 2005), while the long chain (C_{27}-C_{35}) are mainly from higher-plants (Cranwell, 1973; Meyers, 2003; Gao and Chen, 2008). The saturated hydrocarbon from OGIs had dominant peaks of C_{20}-C_{23} and a highest carbon number *n*-alkane of C_{36}, indicating their parent biomass contained high plant input. The 17α(H)-diahopane (C_{30}RH) was considered a possible terrestrial marker because of its

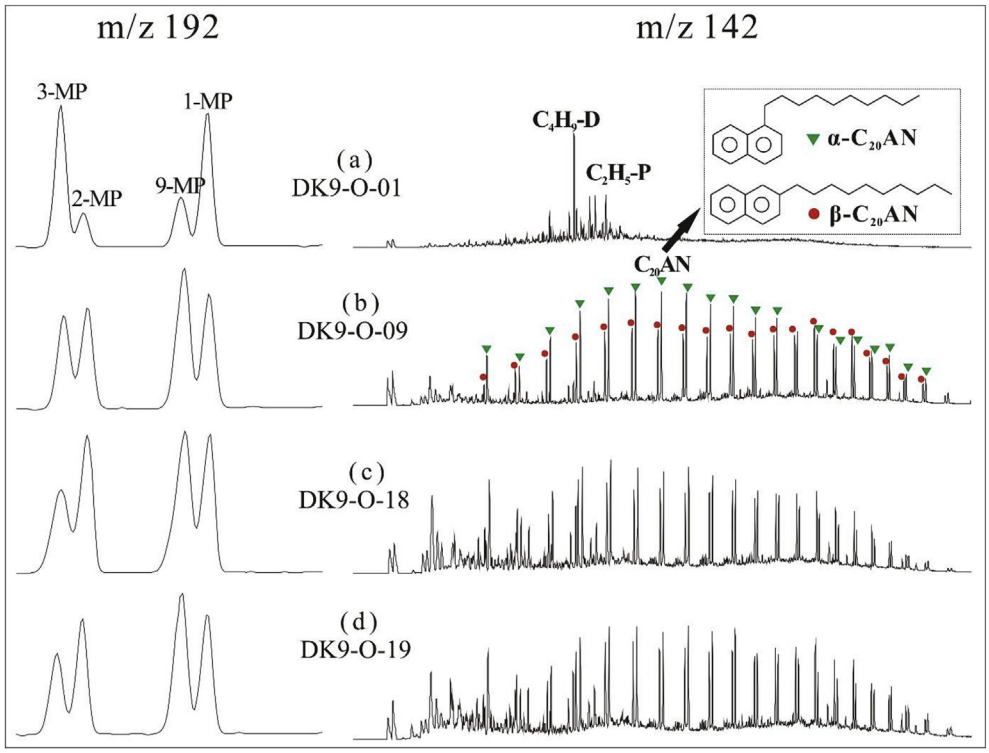

Fig. 8. M/z 192 and m/z142 chromatograms of the aromatic hydrocarbon from OGI. The biomarker assignments are listed in Table 4.

Table 5
Classification of oil and gas indication (OGI).

Type	Biodegradation	Maturity	C_{30}RH	αααRC_{27-29}S	C_{27}DS	M	LCA
I-type	Yes	high	high	low	high	<1	No
II-type	No	low	low	high	low	>1	Yes

Note: C_{30}RH: 17α(H)-diahopane; αααRC_{27-29}S: αααR-C_{27-29} regular sterane; C_{27}DS: C_{27}-diasteranes M = {(2-MP)+(9-MP)}/{(1-MP)+(3-MP)}; LCA: Long-chain alkylnaphthalene.

usual presence in coals, terrestrially source rock, or terrestrially sourced oils (Philip and Gilbert, 1985; Obermajer et al., 2002). The alkylnaphthalene was closely associated with the aromatization of sesquiterpanes or triterpanes from microorganisms or terrestrially sourced plants (Püttmann and Villar, 1987; Strachan et al., 1988; Forster et al., 1989). The biomarkers for 17α(H)-diahopane and the series of alkylnaphthalene detections further confirmed the OGI parent biomass had high plant input.

The presence of the UCM peak and C_{16-31} *n*-alkanes on the chromatogram of DK9-O-01 OGI indicated that these samples generally suffered from biodegradation, while the relative abundance of *n*-alkanes suggests later charging hydrocarbons (Cheng et al., 2015). The ratios of Ts/(Ts + Tm), C_{30}RH/C_{29}Ts, Tricyclics/17α(H)-hopanes, C_{29}-ββ/(αα+ββ), and C_{29}-20S/(20S + 20R), considered as mature parameters (Peters et al., 2005), were higher in the DK9-O-01 OGI than those in the other OGIs, indicating a higher thermal maturity of the DK9-O-01 OGI. The C_{30}RH and C_{29}Ts formations were associated with the catalysis of clay minerals (Peters et al., 2005). Diasteranes was mainly formed from the rearrangement reaction of sterane carbon skeletons under catalysis of clay minerals (De Leeuw et al., 1989), and acidity (low pH) or oxidation conditions would accelerate the diasterane formation (Moldowan et al., 1986; Brincat and Abbott, 2001), while the regular steranes isomerization may also be influenced by clay mineral catalysis (Huang et al., 1990; Seifert and Moldowan, 1986). Therefore, the difference between the DK9-O-01 OGI and the other OGIs for the diahopane, diasterane, and regular sterane isomer distributions may be related to the catalysis or oxidation conditions. Though their parent biomass contained high plant input, the C_{30}RH and long chain alkylnaphthalene were detected in the DK9-O-01 OGI and the other OGIs, which may be related to the parent biomass type, depositional environment, or later geochemistry processes.

According to the above discussion, the OGIs can be classified into two types: the DK9-O-01 sample was one type (marked as I-type), while the other three ones were another one (marked as II-type) (Table 5). The I-type OGI suffered from biodegradation and then received later charging hydrocarbon, featured with relative high maturity, high concentrations of diahopane and diasterane, and M value < 1, but without a series of long chain alkylnaphthalene. In contrast, the II-type OGI did not suffer from biodegradation and had lower concentrations of diahopane, diasterane, and regular sterane αββ isomer than that of I-type, as well as lower maturity and a series of long chain alkylnaphthalenes, with M value > 1.

4.2.2. Oil-to-source correlation of the OGI with Middle Jurassic source rocks

The dichloromethane extracts of source rocks and liquid hydrocarbon products cracked from source rocks at 400 °C were analyzed by GC-MS. The results showed that those source rocks also can be classified into two types (marked as A-type and B-type) based on the biomarker distribution difference (Fig. 9, taking DK9-O-08 and DK9-O-10 as the examples): (1) A-type source rock (Dk9-O-02~DK9-O-08), at a depth of 169–225 m, had C_{13}-C_{30} *n*-alkanes with C_{17} as the dominant component, high concentrations of C_{30}RH and C_{29}Ts, and a V-type distribution of steranes, but their ααα sterane isomers had lower concentrations than their αββ ones. (2) B-type source rock (Dk9-O-10~DK9-O-16), presenting at the depth of 249–301 m, had C_{13}-C_{34} *n*-alkanes with C_{21} or C_{23} as the dominant component, low concentrations of C_{30}RH and C_{29}Ts, and a V-type distribution of steranes, but their ααα sterane isomers had higher concentrations than their αββ ones.

Series of long chain alkylnaphthalenes were detected in the extracts of all source rock, but were only found in the 400 °C cracked products from samples DK9-O-03, DK9-O-11, and DK9-O-14 to DK9-O-16. Therefore, the reason why all A-type source rock extracts contained a series of long chain alkylnaphthalenes could be because some of the A-type source rock was polluted by their neighboring strata.

The triangle of C_{27}-C_{28}-C_{29} regular steranes can be used to divide different parent biomass type (Moldowan et al., 1985), while the triangle of Pr/Ph-Pr/C_{17}-Ph/C_{18} can be used to judge different depositional environments of the parent biomass (Wang et al., 1997). Combining all OGI and source rock samples on the two triangles, the results (Fig. 10) indicate that those samples can be divided into two groups (Group A and Group B) on the Pr/Ph-Pr/

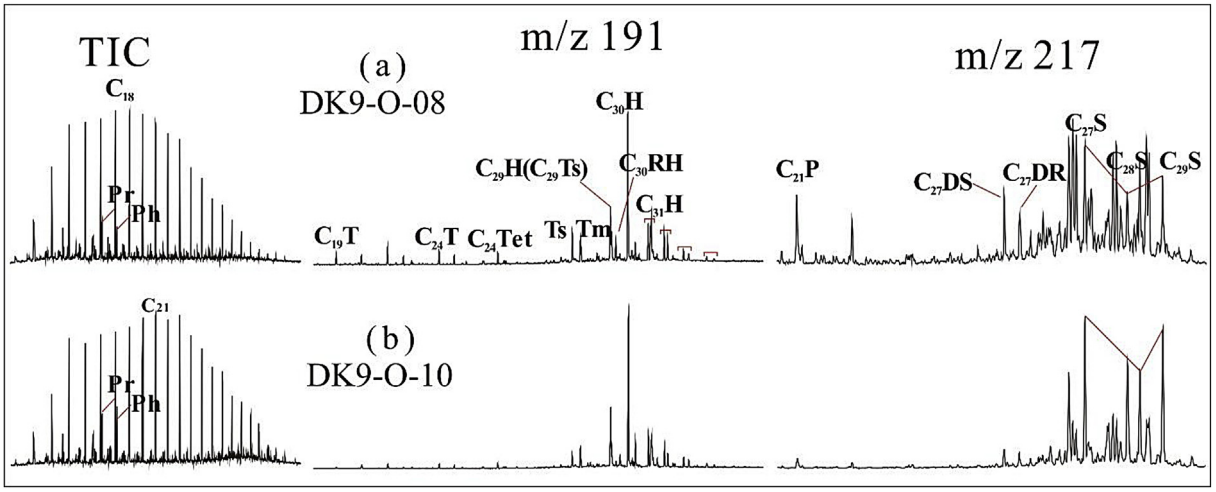

Fig. 9. Chromatograms of *n*-alkanes, terpanes and steranes from dichloromethane extracts of DK9-O-08(a) and DK9-O-10(b) samples. The biomarker assignments are listed in Table 4.

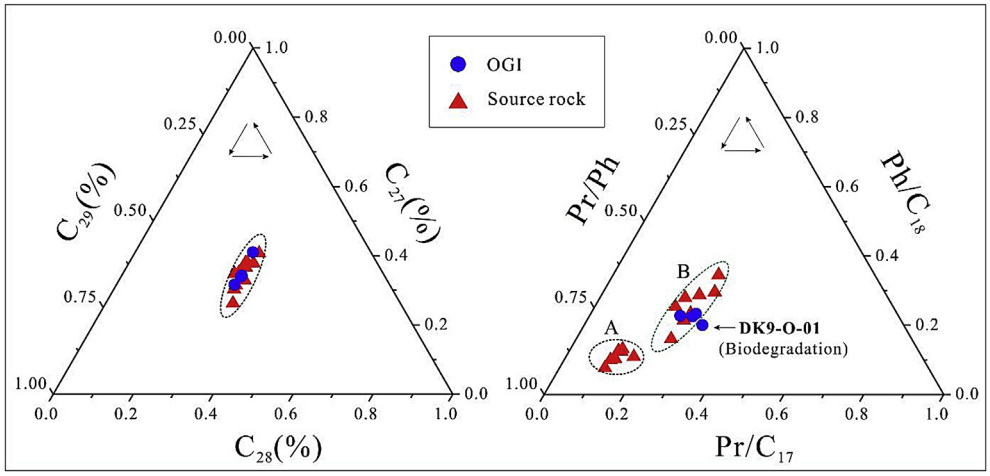

Fig. 10. Triangles of C_{27}-C_{28}-C_{29} regular steranes (left) and Pr/Ph-Pr/C_{17}-Ph/C_{18} (right) from dichloromethane extracts of OGIs and source rocks from DK9 well.

C_{17}-Ph/C_{18} triangle but not on the C_{27}-C_{28}-C_{29} triangle. It seems that the two groups of source rocks had similar parent biomasses, which were formed from different depositional environments. On the Pr/Ph-Pr/C_{17}-Ph/C_{18} triangle, the A-type source rocks were present in the Group A area with Pr/Ph > 70% and Ph/C_{18} < 10%, while the B-type ones and all of OGIs were in the Group B area with Pr/P ranging from 40 to 70% and Ph/C_{18} from 10 to 40%. According to Wang et al. (1997) studies, the parent biomass of the samples from the Group A area (A-Type source rock) were derived from humic organisms from lacustrine and swamp facies, while that of the samples from the Group B area (B-Type source rock) were deposited in a freshwater environment. The OGIs of DK9-O-09, DK9-O-18, and DK9-O-19 had the similar depositional environment to the B-Type source rock, but the DK9-O-01 OGI did not because the *n*-alkanes and isoprenoid compounds from DK9-O-01 suffered biodegradation.

According to the above discussion about *n*-alkanes, C_{30}RH, C_{29}Ts, diasteranes, and regular steranes, the I-type OGI had a similar biomarker distribution feature to the A-type source rocks, while the II-type OGI and B-type source rocks also had a similar distribution. We can therefore conclude that I-type OGI originated from a shallow source rock (A-type, DK9-O-02 to DK9-O-08), while the II-type ones correlated well with the B-type source rocks. The II-type OGIs may originate from the B-type source rocks detected in this paper (DK9-O-010 to DK9-O-16) or from deeper source rocks than the Middle Jurassic strata.

4.3. Parent origination analysis of gas hydrate

4.3.1. Organic geochemistry characteristic of adsorbed gas of rocks

Adsorbed gases from the rocks were obtained when dichloromethane extracted samples (DK9-O-01 to DK9-O-07) were heated to 300 °C for 72 h in the closed glass tube systems, and then their components and stable carbon isotopes were detected. The results (Table 6) showed that the adsorbed gas had very low contents of C_1-C_5 hydrocarbons (0.69%–5.65%) but greater numbers of inorganic gases, including CO_2, H_2, O_2, and N_2. Among the C_1-C_5 hydrocarbons, CH_4 was the dominant component with a content of 35.98%–55.41%, while ethane, or propane, was second with a content of about 20%. The $C_1/(C_2+C_3)$ ratio of adsorbed gases was near 1, except for the DK9-O-02 sample, which has a ratio of 2.14. These gases had drying coefficients of 35.98%–62.88%, indicating they are wet gases. The stable carbon isotope distribution of C_1-C_3 hydrocarbons had $\delta^{13}C_1$ of −46.45 to −30.67‰ (average −38.31‰), $\delta^{13}C_2$ of −39.71 to −32.88‰ (average −35.21‰), and $\delta^{13}C_3$ of −36.29 to −31.90‰ (average −33.09‰). As a whole, the order of carbon isotope value from the adsorbed gases was $\delta^{13}C_1 < \delta^{13}C_2 < \delta^{13}C_3$, showing a normal carbon isotope sequence.

Generally, the organic originated gas had $\delta^{13}C_1 < -30$‰ and $\delta^{13}C_1 < \delta^{13}C_2 < \delta^{13}C_3$ (Burruss and Laughrey, 2010). Though both are considered organic originated gases, the coal-derived gas originated humic parent biomass had $\delta^{13}C_2 > -28.5$‰, but oil-associated gas originated sapropelic ones had $\delta^{13}C_2 < -28.5$‰ (Dai et al., 2014). The adsorbed gas featured a normal carbon isotope sequence for C_1-C_3 hydrocarbon gas, $\delta^{13}C_1 < -30$‰, $\delta^{13}C_2 < -28.5$‰ and $\delta^{13}C_2 < -25$‰, indicating they derived from a sapropelic parent biomass and are oil-associated gases.

4.3.2. Organic geochemistry characteristic of cracked gas of rocks

Plenty of hydrocarbon gases were generated when the rocks were treated at 400 °C for 72 h. The C_1-C_5 hydrocarbon gas contents varied sharply with the lithology or well changing (Table 6). The DK9 well often had relatively high C_1-C_5 contents when compared with the other wells because the rocks from DK9 well were mainly mudstones and oil shales. The maximum ratio of $\sum C_{1\text{-}5}$/Total from sample DK-O-12 even reached 76.5%, but this ratio value was generally very low for the other wells. For example, DK13-11-05 only had a maximum ratio value of 24.15%. However, for the C_1-C_5 relative contents, all of samples displayed the order of $C_1 > C_2 > C_3$.

For the stable carbon isotope distribution of C_1-C_3 hydrocarbons, the cracked gases had $\delta^{13}C_1$ of −40 to −50‰, $\delta^{13}C_2$ of −35 to −20‰, and $\delta^{13}C_3$ of −35 to −20‰, showing a normal carbon isotope sequence ($\delta^{13}C_1 < \delta^{13}C_2 < \delta^{13}C_3$).

4.3.3. Gas-to-gas correlation of the adsorbed and cracked gas of Middle Jurassic source rocks with gas hydrate and drilling core gas

4.3.3.1. Gas components of adsorbed and cracked gas of rock, gas hydrate and core gas. Natural gas can be classified into three types, including organic thermogenic gas, biogenetic gas, and hybrid gas, based on the diagram of $\delta^{13}C_1$–$\{C_1/(C_2+C_3)\}$ (Bernard et al., 1977). Generally speaking, the gas with $\delta^{13}CH_4 < -60$‰ and a R value ($C_1/(C_2+C_3)$) >1000 was microbial gas, and that with $\delta^{13}CH_4 > -50$‰ and R < 100 was thermogenic gas, while the gas with −60‰ < $\delta^{13}CH_4$ < −50‰ and 100 < R < 1000 was hybrid gas (Kvenvolden, 1995). When entering the samples from adsorbed and cracked gases of rocks, gas hydrate (Lu et al., 2011), and core gas (Huang et al., 2011; Liu et al., 2012; He et al., 2015) into the diagram of $\delta^{13}C_1$–$\{C_1/(C_2+C_3)\}$, the results showed that most of the samples appeared to be thermogenic gases, while a few core gases were in

Table 6
The gas components and their stable carbon isotope for adsorbed gas (300 °C) and cracked gas (400 °C) of rocks.

Samples	$\sum C_{1-5}$/Total (%)	$C_1/\sum C_{1-5}$ (%)	$C_2/\sum C_{1-5}$ (%)	$C_3/\sum C_{1-5}$ (%)	$C_1/(C_2+C_3)$	$\delta^{13}C_1$ (‰)	$\delta^{13}C_2$ (‰)	$\delta^{13}C_3$ (‰)
Adsorbed gas (300°C)								
DK9-O-01	4.42	35.98	17.85	19.85	0.95	−46.45	−39.71	−36.29
DK9-O-02	3.40	62.88	17.22	12.15	2.14	−37.79	−34.61	−31.90
DK9-O-03	5.65	40.24	17.88	19.66	1.07	−38.87	−32.88	−32.30
DK9-O-04	0.69	51.04	22.36	15.08	1.36	−39.17	−34.04	−32.97
DK9-O-06	/	54.21	25.48	11.92	1.45	−30.67	−36.94	/
DK9-O-07	1.21	55.41	22.42	13.85	1.53	−36.93	−33.06	−32.01
Cracked gas (400°C)								
DK9-O-01	34.35	45.49	22.20	16.39	1.18	−43.61	−34.63	−32.45
DK9-O-03	41.92	37.41	26.33	21.11	0.79	−44.52	−36.19	−32.01
DK9-O-04	17.18	48.53	22.38	15.08	1.30	−43.38	−33.88	−32.60
DK9-O-06	35.41	44.95	22.63	16.93	1.14	−40.00	−33.79	−32.21
DK9-O-07	36.02	46.70	22.70	16.31	1.20	−41.42	−33.82	−31.40
DK9-O-09	12.85	47.77	22.31	15.32	1.27	−42.73	−33.69	−31.51
DK9-O-10	33.28	81.13	16.04	2.55	4.36	−39.43	−29.38	−27.62
DK9-O-11	61.19	38.15	24.97	20.77	0.83	\	\	\
DK9-O-12	76.50	39.95	24.76	19.75	0.90	−43.87	−36.57	−34.06
DK9-O-13	63.51	42.98	26.97	19.22	0.93	−45.29	−38.67	−35.06
DK9-O-16	24.62	39.91	25.13	19.22	0.90	−49.91	−39.26	−37.01
DK9-O-17	1.36	71.00	16.61	7.42	2.95	−35.68	−25.69	−25.42
DK9-O-18	28.31	59.42	21.34	12.01	1.78	−35.03	−55.92	−27.49
DK9-O-19	19.15	49.88	22.84	15.42	1.30	\	\	\
DK10-16-01	1.46	32.57	14.47	16.16	1.06	−48.81	−35.84	−34.54
DK10-16-02	/	/	/	/	/	−47.26	−35.96	−34.93
DK10-16-03	9.97	46.51	22.93	18.51	1.12	−48.74	−39.81	−38.45
DK10-16-04	1.05	14.13	14.80	26.05	0.35	−47.20	−42.25	−39.72
DK11-14-01	4.98	33.33	17.44	16.97	0.97	−40.55	−32.15	−30.33
DK11-14-02	2.95	26.94	15.79	17.03	0.82	−42.85	−32.60	−31.09
DK11-14-03	1.15	25.76	13.75	18.96	0.79	−43.90	−33.39	−33.21
DK11-14-04	5.48	46.30	23.55	19.02	1.09	−44.78	−37.96	−36.23
DK11-14-05	14.06	58.47	20.46	14.03	1.70	−36.86	−28.32	−28.82
DK11-14-06	7.98	46.47	24.40	18.74	1.08	−44.83	−36.02	−34.79
DK11-14-07	12.82	36.66	23.33	22.91	0.79	−46.90	−38.08	−35.27
DK12-13-01	3.00	23.72	13.12	19.14	0.74	−47.53	−36.88	−35.57
DK12-13-02	8.12	42.62	25.59	21.25	0.91	−45.14	−38.19	−35.69
DK12-13-03	5.95	40.43	24.82	21.30	0.88	−45.67	−38.43	−35.83
DK12-13-04	13.71	43.05	23.25	18.41	1.03	−44.16	−36.74	−34.34
DK12-13-05	2.45	43.29	24.92	20.00	0.96	−44.71	−38.12	−35.90
DK12-13-06	3.91	42.08	23.96	21.05	0.93	−46.05	−38.75	−36.61
DK12-13-07	6.69	42.56	24.62	22.10	0.91	−45.78	−38.49	−36.21
DK12-13-08	1.69	44.42	23.72	19.81	1.02	−45.53	−38.71	−35.97
DK12-13-09	15.66	37.98	24.36	19.22	0.87	−50.87	−40.02	−37.87
DK13-11-01	1.08	41.27	14.81	17.73	1.27	−43.57	−36.90	−33.97
DK13-11-02	14.79	35.14	25.50	22.66	0.73	−49.28	−40.11	−37.40
DK13-11-03	15.03	45.32	23.85	17.98	1.08	−44.34	−36.99	−35.03
DK13-11-04	0.27	38.73	42.66	12.40	0.70	−48.02	−37.87	−35.61
DK13-11-05	24.15	34.86	48.89	12.00	0.57	−52.67	−41.87	−40.26
DK13-11-06	4.94	43.27	35.05	14.47	0.87	−44.05	−33.17	−32.10
DK13-11-07	1.99	43.73	27.49	17.69	0.97	−43.04	−33.03	−32.98
DK13-11-08	0.16	30.62	24.05	20.22	0.69	−44.01	−34.17	−33.63
DK13-11-09	1.17	31.17	35.88	18.59	0.57	−35.81	−31.64	−32.06

the mixed gas area (Fig. 11). Most of the cracked gas had a $C_1/(C_2+C_3)$ ratio around 1 and was located at the bottom of thermogenic gas area, while the adsorbed gas, gas hydrate, and part of the core gas had $C_1/(C_2+C_3)$ ratios of 1–10, which are located in the middle of this area. The other core gases appeared at the top or out of this area.

When taking the four kinds of gas from Fig. 11 and entering them into the C_1-C_2-C_3 triangle and $\ln(C_1/C_2)$-$\ln(C_2/C_3)$ diagram, we found those gases can be classified into two groups: (1) the adsorbed and cracked gases and (2) the gas hydrate and core gas (Figs. 12 and 13). On the C_1-C_2-C_3 triangle, the adsorbed and cracked gases are located near the area where $50\% < C_1 < 100\%$, $20\% < C_2 < 50\%$, and $0 < C_3 < 37.5\%$, obviously different from the gas hydrate and core gas with $25\% < C_1 < 62.5\%$, $20\% < C_2 < 50\%$, and $0 < C_3 < 37.5\%$. On the $\ln(C_1/C_2)$-$\ln(C_2/C_3)$ diagram, the group of adsorbed and cracked gases had $-0.2 < \ln(C_1/C_2) < 0.6$, while the other ones had $\ln(C_1/C_2) > 0.6$.

The difference in the C_1-C_3 components between the adsorbed and cracked gases and the gas hydrate and core gas can be explained in three cases: (1) They had a different parent biomass; (2) The adsorbed and cracked gases originated from kerogen degradation, while the gases of gas hydrate and core gas were mainly from oil cracking (Tian et al., 2007; Wang et al., 2013). (3) The Gas composition differentiated during the natural formation of gas hydrate (Lin and Zeng, 2010).

4.3.3.2. Stable carbon isotope of C_1-C_3 gases from adsorbed and cracked gas of rock, gas hydrate and core gas. When taking the samples of adsorbed and cracked gases, gas hydrate (Lu et al., 2011), core gas (Huang et al., 2011; Liu et al., 2012; He et al., 2015), and coalbed gas (Cao et al., 2012) into the diagrams of $\delta^{13}C_1$-$\delta^{13}C_2$, $\delta^{13}C_2$-$\delta^{13}C_3$ and $\delta^{13}C_1$-$\delta^{13}C_3$, we found the following results: (1) All samples, except those for the coalbed gas, were closely distributed in the same area and difficult to separate on the

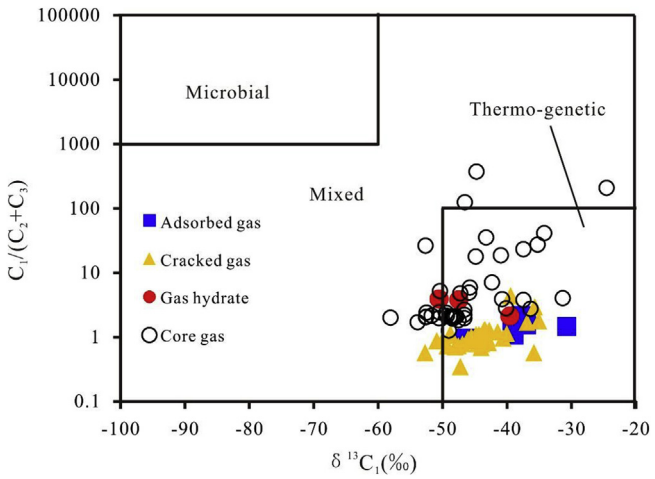

Fig. 11. Diagram of $\delta^{13}C_1$-{$C_1/(C_2+C_3)$}. Note: The gas hydrate data were from Lu et al. (2011); The core gas data were from Huang et al. (2011), Liu et al. (2012) and He et al. (2015).

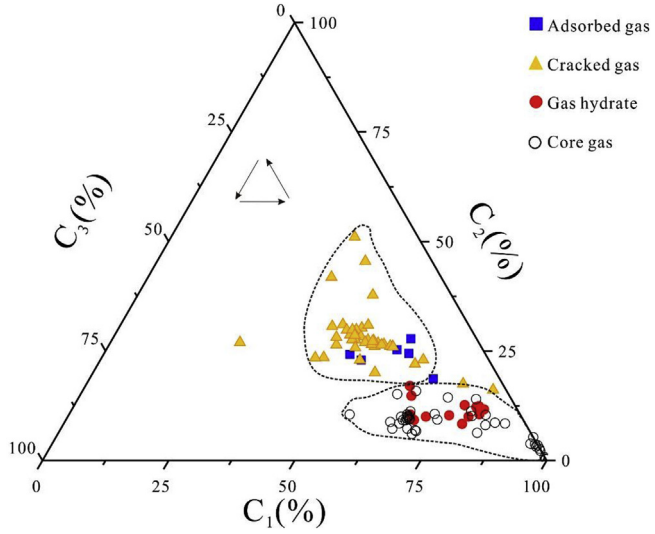

Fig. 12. Triangles for C_1-C_2-C_3 hydrocarbon gas from adsorbed and cracked gases, and gas hydrate and core gas. Note: The gas hydrate data are from Lu et al. (2011); The core gas data are from Huang et al. (2011), Liu et al. (2012) and He et al. (2015).

$\delta^{13}C_1$-$\delta^{13}C_2$ diagram (Fig. 14a). The coalbed gases were located far away from this area because they had a heavier ethane enriched carbon isotope, $\delta^{13}C_2 > -20‰$. (2) The samples of adsorbed and cracked gases, gas hydrate, and core gas displayed a positive linear distribution on the $\delta^{13}C_2$-$\delta^{13}C_3$ diagram (Fig. 14b). Linear fitting was done for those points based on the data of $\delta^{13}C_2$ and $\delta^{13}C_3$ using Excel software and the R^2 value (R-squared) was 0.8075, showing those samples have good correlation. (3) On the $\delta^{13}C_1$-$\delta^{13}C_3$ diagram (Fig. 14c), the gas hydrate and core gas distributed near the adsorbed and cracked gases as a whole. However, a little differentiation was still observed with a $\delta^{13}CH_4$ of $< -45‰$. On the area of $\delta^{13}CH_4 < -45‰$, the samples of gas hydrate and core gas (E1 area) had a heavier stable carbon isotope than that of cracked gas (E2 area).

On the diagrams of $\delta^{13}C_1$-$\delta^{13}C_2$, $\delta^{13}C_2$-$\delta^{13}C_3$ and $\delta^{13}C_1$-$\delta^{13}C_3$, all samples, except those for coalbed gas, had good correlation, indicating that they had a similar parent biomass as the Middle Jurassic source rocks. The coalbed gases often had heavier methane and ethane enriched carbon isotope than the other gases, showing not necessary correlation with the gas hydrate and core gas, which was consistent with prior studies (Huang et al., 2011; Lu et al., 2013a,c). Compared with the diagrams for $\delta^{13}C_1$-$\delta^{13}C_2$ and $\delta^{13}C_2$-$\delta^{13}C_3$, the third diagram displayed partial differentiation. The direct reason for this phenomenon was that the subject matter (CH_4 and C_3H_8) used for the $\delta^{13}C_1$-$\delta^{13}C_3$ diagram had a two carbon number difference, while those on the diagrams of $\delta^{13}C_1$-$\delta^{13}C_2$, $\delta^{13}C_2$-$\delta^{13}C_3$ were only one carbon number. However, the fundamental reason may be that the gas hydrate and core gas underwent a different formation process than the cracked gas. The cracked gas generated in closed glass tube systems can be regarded as a kerogen cracked gas, with no gas component differentiation. However, the gas of gas hydrate and core gas experienced the differentiation process and their organic matter origination (kerogen or oil) were still uncertain. Lu et al. (2015a) even speculated the gas hydrate and core gas were derived from oil thermal degradation. In other words, the gas hydrate and core gas had a similar parent biomass type but a different formation process than the cracked gas.

4.3.3.3. Possible source rocks of gas hydrate. According to the above discussion, the gas hydrate and core gas had a similar parent biomass as the Middle Jurassic source rocks, but a different formation process from the cracked gas. Additionally, the Middle Jurassic source rocks did not have high maturity (did not reach the wet gas stage) and cannot support enough hydrocarbon gases for

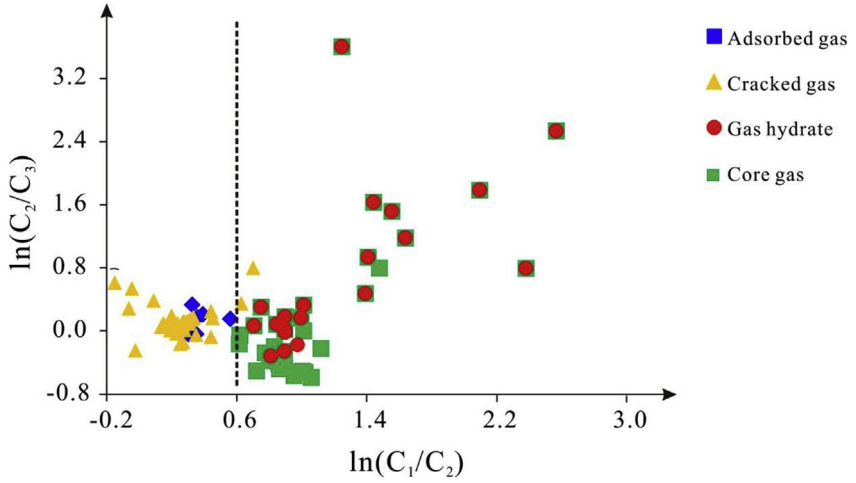

Fig. 13. Diagram of $\ln(C_1/C_2)$-$\ln(C_2/C_3)$ from adsorbed and cracked gases, and gas hydrate and core gas. Note: The gas hydrate data are from Lu et al. (2011); The core gas data are from Huang et al. (2011), Liu et al. (2012) and He et al. (2015).

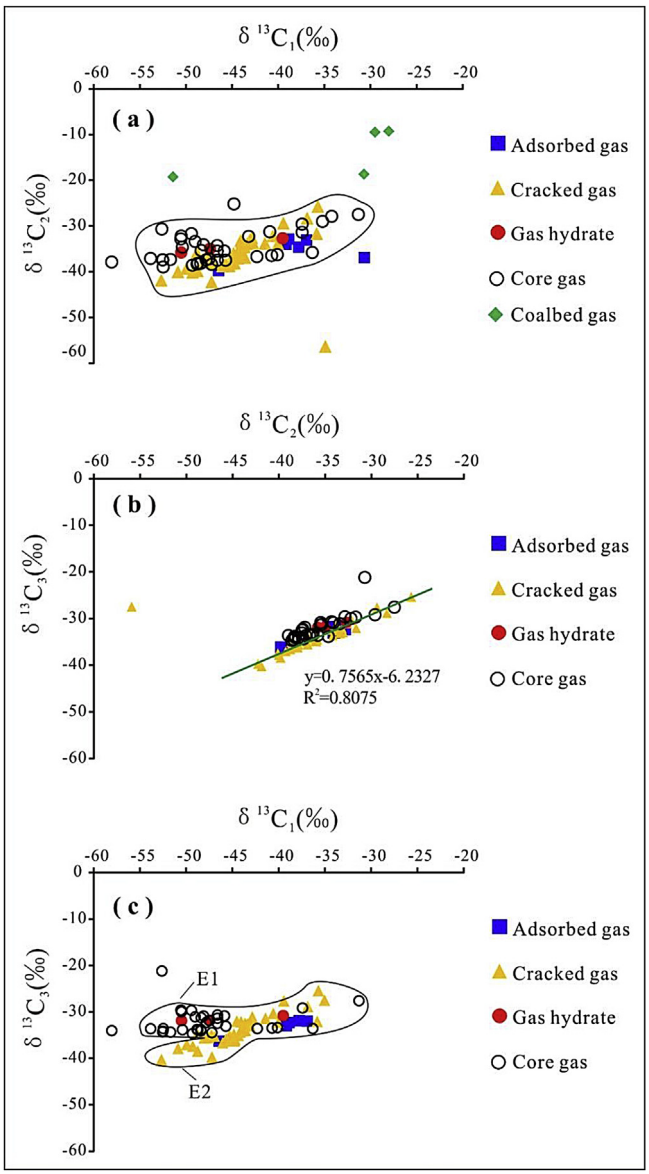

Fig. 14. Diagrams of $\delta^{13}C_1$-$\delta^{13}C_2$ (a), $\delta^{13}C_2$-$\delta^{13}C_3$ (b) and $\delta^{13}C_1$-$\delta^{13}C_3$ (c) from adsorbed and cracked gases, gas hydrate and core gas. Note: The gas hydrate data are from Lu et al. (2011); The core gas data are from Huang et al. (2011), Liu et al. (2012), and He et al. (2015); The coalbed gas data are from Cao et al. (2012).

gas hydrate. Therefore, the source rocks of gas hydrate and core gas may be mainly from deeper strata.

Similar to the Middle Jurassic source rocks, the parent biomass of the gas hydrate and core gas should be deposited in a fresh water environment, which is consistent with Liu et al. (2012) and He et al. (2015). Since the Sinian period, the South Qilian area has experienced the process of paleo-ocean-basin closure→uplift→erosion twice (Fu and Zhou, 1998) that can form fresh water depositional environments. The first occurred during the Late Silurian under the effects of the Caledonian Movement. However, the South Qilian area began to sink and formed a wide shallow-marine shelf facies in the Carboniferous. The second occurrence happened at the terminal of the Late Triassic under the influence of the Indosinian Movement. Therefore, the strata from the Late Silurian to Carboniferous or after Later Triassic were the possible source rocks for the gas hydrate and core gas. There are three sets of source rocks deposited during the two periods, including Carboniferous dark mudstone (limestone), Galedeshi Formation dark mudstone from the upper Triassic, and Jurassic dark shale. It seems that the source rocks of the gas hydrate and core gas may be from the Later Triassic-Early Jurassic strata or Carboniferous strata.

The II-type OGI, also possibly originated from deeper strata, were closely accompanied with gas hydrate in the drilling well and had a similar parent biomass and depositional environment as the gas hydrate, showing they have close correlation in hydrocarbon origin.

5. Conclusions

The Middle Jurassic source rocks with gas hydrate were mainly type I-II kerogens, stayed at a low-mature stage, and belonged to a high quality source rock.

The parent biomass of OGI contained high plant input and was likely deposited in a freshwater and enriched clay mineral environment. Those OGI can be classified into two types based on their biomarker features. The first type (I-type) suffered from biodegradation and then received later charging hydrocarbon, featuring relatively high maturity, high concentrations of diahopane, diasterane, and regular sterane αββ isomer, and a M ({(2-MP)+(9-MP)}/{(1-MP)+(3-MP)}) value < 1, but lacked a series of long chain alkylnaphthalene. In contrast, the II-type one did not suffer from biodegradation, and it had low maturity and lower concentrations of diahopane, diasterane, and regular sterane αββ isomer than that of I-type, with an abundance of long chain alkylnaphthalenes, but a M value > 1. The I-type OGI originated from upper Middle Jurassic source rocks, while the II-type one was derived from the bottom of the Middle Jurassic or even deeper source rocks.

The adsorbed gas (300 °C) of the Middle Jurassic rocks was very wet, had a normal carbon isotope sequence, and can be regarded as an organic thermogenic gas derived from Middle Jurassic source rocks. The cracked gas (400 °C) of the Middle Jurassic rocks had a C_1-C_3 content with $C_1 > C_2 > C_3$, $\delta^{13}C_1$ of −50‰ to −40‰, $\delta^{13}C_2$ of −40‰ to −30‰, and $\delta^{13}C_3$ of −35‰ to −20‰, displaying a normal carbon isotope sequence ($\delta^{13}C_1 < \delta^{13}C_2 < \delta^{13}C_3$). The gas hydrate and core gas had a similar parent biomass as the Middle Jurassic source rocks, but a different formation process from the cracked gas.

The II-type OGI, also possibly originated from deeper strata, were closely accompanied by gas hydrate in the drilling well and had a similar parent biomass and depositional environment as gas hydrate, showing they have close correlation on hydrocarbon origin.

Acknowledgments

This work has been financially supported by the National Program for Gas hydrate Exploration and Test-production (GZHL20110310, GZH201400302, DD20160223) and the Project (2013002) invested by Shenhua Qinghai Energy Development Co., Ltd.

References

Bernard, B., Brooks, J.M., Sackett, W.M., 1977. A geochemical model for characterization of hydrocarbon gas sources in marine sediments. In: Proceeding of 9th Annual Offshore Technology Conference. Offshore Technology Conference, Houston, pp. 435–438.

Blumer, M., Guillard, R.P.L., Chase, T., 1971. Hydrocarbons of marine phytoplankton. Mar. Biol. 8 (3), 183–189.

Boswell, R., Collett, T.S., 2011. Current perspectives on gas hydrate resources. Energy Environ. Sci. 4, 1206–1215.

Brincat, D., Abbott, G.D., 2001. Some aspects of the molecular biogeochemistry of massive and laminated rocks from Naples Beach section (Santa Barbara-Ventura basin). In: Isaacs, C.M., Rullkoetter, J. (Eds.), The Monterey Formation: from

Rocks to Molecules. Columbia University Press, New York, pp. 140–149.
Burruss, R.C., Laughrey, C.D., 2010. Carbon and hydrogen isotopic reversals in deep basin gas: evidence for limits to the stability of hydrocarbons. Org. Geochem. 41 (12), 1285–1296.
Cao, D., Wang, D., Li, J., Dou, X., 2012. Gas source analysis of natural gas hydrate of Muri coalfield in Qilian Mountain permafrost, Qinghai Province, China. J. China Coal Soc. 37 (8), 1364–1368 (in Chinese with English abstract).
Cheng, B., Liao, Z., Wang, T., Liu, H., Tian, Y., Yang, S., 2015. Multiple charges to Sinian reservoirs in the middle Sichuan basin, SW China: insight from the adsorbed/occluded hydrocarbons in solid bitumens. J. Pet. Sci. Eng. 127, 359–366.
Cranwell, P.A., 1973. Chain-length distribution of *n*-alkanes from lake sediments in relation to post-glacial environmental change. Freshw. Biol. 3 (3), 259–265.
Cranwell, P.A., Eglinton, G., Robinson, N., 1987. Lipids of aquatic organisms as potential contributors to lacustrine sediment-II. Org. Geochem 11 (6), 513–527.
Dai, J., Gong, D., Ni, Y., Huang, S., Wu, W., 2014. Stable carbon isotopes of coal-derived gases sourced from the Mesozoiccoal measures in China. Org. Geochem. 74, 123–142.
De leeuw, J.M., Cox, H.C., Van Grass, G., Van De Meer, F.W., Peakman, T.M., Baas, J.M.A., Van De Graaf, B., 1989. Limited double bond isomerisation and selective hydrogenation of steranes during early diagenesis. Geochim. Cosmochim. Acta 53, 903–909.
Ficken, K.J., Li, B., Swain, D.L., Eglinton, G., 2000. An *n*-alkane proxy for the sedimentary input of submerged/floating freshwater aquatic macrophytes. Org. Geochem 31 (7–8), 745–749.
Forster, P.G., Alexander, R., Kagi, R.I., 1989. Identification and analysis of tetramethylnaphthalenes in petroleum. J. Chromatogr. A 483, 384–389.
Fu, J., Zhou, L., 1998. Carboniferous-Jurassic stratigraphic provinces of the southern Qilian Basin and their petro-geological features. Northwest Geosci. 19 (2), 47–54 (in Chinese with English abstract).
Gao, X., Chen, S., 2008. Petroleum pollution in surface sediments of Daya Bay, South China, revealed by chemical fingerprinting of aliphatic and alicyclic hydrocarbons. Estuar. Coast. Shelf S 80 (1), 95–102.
Gao, G., Zhang, W., Xiang, B., Liu, G., Ren, J., 2016. Geochemistry characteristics and hydrocarbon-generating potential of lacustrine source rock in Lucaogou formation of the Jimusaer Sag, Junggar basin. J. Pet. Sci. Eng. 145, 168–182.
He, X., Liu, C., Meng, Q., Lu, Z., Wen, H., Li, Y., Zhang, S., Wang, J., 2015. Gas composition of hydrate-bearing cores in Juhugeng drilling area in Qinghai and its indicative significance. Geoscience 29 (5), 1194–1200 (in Chinese with English abstract).
Huang, D., Li, J., Zhang, D., 1990. Maturation sequence of continental crude oils in hydrocarbon basins in China and its significance. Org. Geochem. 16, 521–529.
Huang, X., Zhu, Y., Wang, P., Guo, X., 2011. Hydrocarbon gas composition and origin of core gas from the gas hydrate reservoir in Qilian Mountain permafrost. Geol. Bull. China 30 (12), 1851–1856 (in Chinese with English abstract).
Kvenvolden, K.A., 1995. A review of geochemistry of methane in nature gas hydrate. Org. Geochem. 23 (11/12), 997–1008.
Lin, X., Zeng, J., 2010. Gas composition differentiation during natural gas hydrate formation and its geological significance. Geoscience 24 (6), 1157–1163 (in Chinese with English abstract).
Liu, C., He, X., Meng, Q., Ye, Y., Zhu, Y., Lu, Z., 2012. Carbon and hydrogen isotopic compositions characteristics of the released gas from natural gas hydrates in the Qilian Mountain Permafrost. Rock Min. Anal. 31 (3), 489–494 (in Chinese with English abstract).
Lu, S., 2015. A global survey of gas hydrate development and reserves: Specifically in the marine field. Renew. Sust. Energy Rev. 41 (1), 884–900.
Lu, Z., Zhu, Y., Zhang, Y., Wen, H., Li, Y., Jia, Z., Liu, C., Wang, P., Li, Q., 2010. Basic geological characteristics of gas hydrates in Qilian Mountain permafrost area, Qinghai province. Min. Depos. 29 (1), 182–191 (in Chinese with English abstract).
Lu, Z., Zhu, Y., Zhang, Y., Wen, H., Li, Y., Liu, C., 2011. Gas hydrate occurrences in the Qilian mountain permafrost, Qinghai province, China. Cold Reg. Sci. Technol. 66 (2–3), 93–104.
Lu, Z., Zhu, Y., Liu, H., Zhang, Y., Jin, C., Huang, X., Wang, P., 2013a. Gas source for gas hydrate and its significance in the Qilian Mountain permafrost. Qinghai Mar. Pet. Geol. 43, 341–348.
Lu, Z., Zhu, Y., Liu, H., Zhang, Y., Wang, P., Huang, X., 2013b. Oil and gas indications at gas hydrate-bearing intervals in the Qilian Mountain Permafrost. Geoscience 27 (1), 231–238 (in Chinese with English abstract).
Lu, Z., Xue, X., Liao, Z., Liu, H., 2013c. Source rocks for gases from gas hydrate and their burial depth in the Qilian Mountain Permafrost, Qinghai: results from thermal stimulation. Energy Fuels. 27 (12), 7233–7244.
Lu, Z., Zhai, G., Wen, H., Li, Y., Wang, W., Zhu, Y., 2015a. Geological constraints on gas hydrate formation and distribution in Sanlutian permafrost of Muli, Qinghai. Geoscience 29 (5), 1002–1013 (in Chinese with English abstract).
Lu, Z., Rao, Z., He, J., Zhu, Y., Zhang, Y., Liu, H., Wang, T., Xue, X., 2015b. Geochemistry of drill core headspace gases and its significance in gashydrate drilling in Qilian Mountain permafrost. J. Asian Earth Sci. 98, 126–140.
Mead, R., Xu, Y., Chong, J., Jaffe, R., 2005. Sediment and soil organic matter source assessment as revealed by the molecular distribution and carbon isotopic composition of *n*-alkanes. Org. Geochem. 36 (3), 363–370.
Meyers, P.A., 2003. Applications of organic geochemistry to paleolimnological reconstructions: a summary of examples from the Laurentian Great Lakes. Org. Geochem. 34 (2), 261–289.
Milkov, A.V., 2004. Global estimates of hydrate-bound gas in marine sediments: how much is really out there? Earth Sci. Rev. 66 (3–4), 183–197.
Moldowan, J.M., Seifert, W.K., Gallegos, E.J., 1985. Relationship between petroleum composition and depositional environment of petroleum source rocks. AAPG Bull. 69 (8), 1255–1268.
Moldowan, J.M., Sundararaman, P., Schoell, M., 1986. Sensitivity of biomarker properties to depositional environment and/or source input in the lower Toarcian of S.W. Germany. Org. Geochem. 10, 915–926.
Moridis, G.J., Collett, T.S., Pooladi-Darvish, M., HanCock, S., Santamarina, C., Boswell, R., Kneafsey, T., Rutqvist, J., Kowalsky, M.B., Reagan, M.T., Sloan, E.D., Sum, A.K., Koh, C.A., 2011. Challenges, uncertainties, and issues facing gas production from gas-hydrates deposits. SPE Reserv. Eval. Eng. 14 (1), 76–112.
Obermajer, M., Osadetz, K.G., Fowler, M.G., Silliman, J., Hansen, W.B., Clark, M., 2002. Delineating compositional variabilities among crude oils from central Montana, USA, using light hydrocarbon and biomarker characteristics. Org. Geochem. 33, 1343–1359.
Peng, J., Pang, X., Shi, H., Peng, H., Xiao, S., Yu, Q., Wu, L., 2016. Hydrocarbon generation and expulsion characteristics of Eocene source rocks in the Huilu area, northern Pearl River Mouth basin, South China Sea: implications for tight oil potential. Mar. Pet. Geol. 72, 463–487.
Peters, K.E., Walters, C.C., Moldowan, J.M., 2005. The Biomarker Guide. In: Biomarker and Isotopes in Petroleum Exploration and Earth History, vol. 2. Cambridge University Press, Cambridge.
Philip, R.P., Gilbert, T.D., 1985. Biomarker distribution in oils predominantly derived from terrigenous source material. In: LeythaeuserD, Rullkotter, J. (Eds.), Advances in Organic Geochemistry. Pergamon Press, Oxford, pp. 73–84.
Püttmann, W., Villar, H., 1987. Occurrence and geochemical significance of 1,2,5,6-tetramethylnaph-thalene. Geochim. Cosmochim. Acta 51, 3023–3029.
Qi, B., Hu, D., Yang, X., Zhang, Y., Tan, C., Zhang, P., Feng, C., 2016. Apatite fission track study of the Cretaceous–Cenozoic stepwise uplift of the middle segment of the Qilian Mountain. Acta Geosci. Sin. 37 (1), 46–58 (in Chinese with English abstract).
Ruppel, C., 2011. Methane hydrates and the future of natural gas. In: MITEI Natural Gas Report, Supplementary Paper on Methane Hydrates, vol. 4, pp. 1–25.
Seifert, W.K., Moldowan, J.M., 1986. Use of biological markers in petroleum exploration. In: Johns, R.B. (Ed.), Methods Geochem. Geophys. 24, 261–290.
Silliman, J.E., Schelske, C.L., 2003. Saturated hydrocarbons in the sediments of lake Apopka, Florida. Org. Geochem. 34 (2), 253–260.
Sloan, E.D., Koh, C.A., 2008. Clathrate Hydrates of Natural Gases, third ed. CRC Press of Tayor & Francis Group, New York, pp. 1–721.
Strachan, M.G., Alexander, R., Kagi, R.I., 1988. Trimethylnaphthalenes in crude oils and sediments: effects of source and maturity. Geochim. Cosmochim. Acta 52, 1255–1264.
Tang, S., Lu, Z., Rao, Z., Wang, T., Tan, P., Liu, H., 2015. The indicative significance of gas composition and isotopes of headspace gases from the gas hydrate drilling core in the Qilian Mountain permafrost: a case study of well DK-9. Geol. Bull. China 34 (5), 961–971 (in Chinese with English abstract).
Tian, H., Xiao, X., Wilkins, R.W.T., Li, X., Gan, H., 2007. Gas sources of the YN2 gas pool in the Tarim Basin-evidence from gas generation and methane carbon isotope fractionation kinetics of source rocks and crude oils. Mar. Pet. Geol. 24, 29–41.
Wang, T., Zhong, N., Hou, D., Huang, G., Bao, J., Li, X., 1997. Genetic Mechanism and Occurrence of Immature Hydrocarbons. Petroleum Industry Press, Beijing, pp. 1–228.
Wang, Q., Lu, H., Greenwood, P., Shen, C., Liu, J., Peng, P., 2013. Gas evolution during kerogen pyrolysis of Estonian Kukersite shale in confined gold tube system. Org. Geochem. 65, 74–82.
Wang, P., Huang, X., Pang, S., Zhu, Y., Lu, Z., Zhang, S., Liu, H., Yang, K., Li, B., 2015. Geochemical dynamics of the gas hydrate system in the Qilian mountain permafrost, Qinghai, Northwest China. Mar. Pet. Geol. 59, 72–90.
Wen, H., Lu, J., Shang, L., Liu, T., Chen, H., Ju, Q., Shao, L., 2006. A sequence stratigraphic discussion of the Jurassic coal measures in the Juhugeng Coalmine area in Qinghai Province. Coal Geol. China 18 (5), 19–21 (in Chinese with English abstract).
Yang, Z., Wang, W., Shao, L., Liu, W., Lü, J., Li, Y., Wen, H., 2015. Depositional environments of the Middle Jurassic in the Sanlutian mining field of the Juhugeng mining area in Qinghai province. Geoscience 29 (5), 1073–1086 (in Chinese with English abstract).
Zhu, Y., Liu, Y., Zhang, Y., 2006. Formation conditions of gas hydrates in permafrost of the Qilian Mountains. Northwest China. Geol. Bull. China 25 (1–2), 58–63 (in Chinese with English abstract).
Zhu, Y., Zhang, Y., Wen, H., Lu, Z., Wang, P., 2010. Gas hydrates in the Qilian Mountain permafrost and their basic characteristics. Acta Geosci. Sin. 31 (1), 7–16 (in Chinese with English abstract).